The model of iron properties for plate impact and explosive compression simulations

Journal of Physics: Conference Series **1556** (2020) 012032 doi:10.1088/1742-6596/1556/1/012032

The model of iron properties for plate impact and explosive compression simulations

S A Dyachkov[1,2], D K Ilnitsky[1], A N Parshikov[1,2] and V V Zhakhovsky[1]

[1] Dukhov Automatics Research Institute (VNIIA), Federal State Unitary Enterprise, Sushchevskaya 22, Moscow 127055, Russia

[2] Joint Institute for High Temperatures of the Russian Academy of Sciences, Izhorskaya 13 Bldg 2, Moscow 125412, Russia

E-mail: serj.dyachkov@gmail.com

Abstract. The material model of iron and steel is developed for fluid dynamics simulations of samples under extreme loading induced by an impact or explosion. The model is validated on a set of plate impact tests using the contact smoothed particles hydrodynamics method. The model takes into account the polymorphic α–ε phase transition in iron which is shown to be correctly reproduced, including the hysteresis effect at unloading. The equation of state for steel is shown to be very close to that of iron on a set of tests with spherical shells under explosive compression; however the yield strength of steel is greater.

1. Introduction

The behavior of iron in extreme conditions has been actively studied since 1950. Both the plastic and thermodynamic properties are important to model this material in various applications. Plastic properties of materials are now possible to obtain directly from large scale molecular dynamics simulations [1] and dislocation dynamics. However, for the considered here pressures of tens of GPa a more simple model seems to be enough.

Nowadays, the four solid phases of iron are known [2]: α (bcc), γ (fcc), δ (bcc), ε (hcp). In standard conditions, iron exists in the α-phase. At the Curie point ($T = 1042$ K) the abrupt change in magnetic properties is observed which is followed by the formation of the γ-phase at 1184 K. Just after the melting there is a region where the δ-phase exists.

The α–ε phase transition appears at $P \approx 13$ GPa which was discovered in shock experiments [3,4]. In particular, its detailed study is performed using the set of plate impact experiments [5]. All the wave profiles obtained via the velocity interferometer system for any reflector (VISAR) measurements of free surface demonstrate the existence of elastic precursor which corresponds the yield strength of $Y \approx 0.5$ GPa. It is followed by the α–ε phase transition front, behind which a mixture of phases exists. The authors notice that the reverse phase transition appears at pressure lower than 13 GPa and may be directly observed in some wave profiles.

In this paper we focus on the iron model development for average compressions of 10–50 GPa which are typical for impact and explosive experiments. The α–ε phase transition with hysteresis is taken into account, while the elastic-plastic behavior is simulated using the most simple case of constant yield strength. Simulations are performed using smoothed particles hydrodynamics (SPH) method with the Riemann problem solution at interparticle contacts [6].

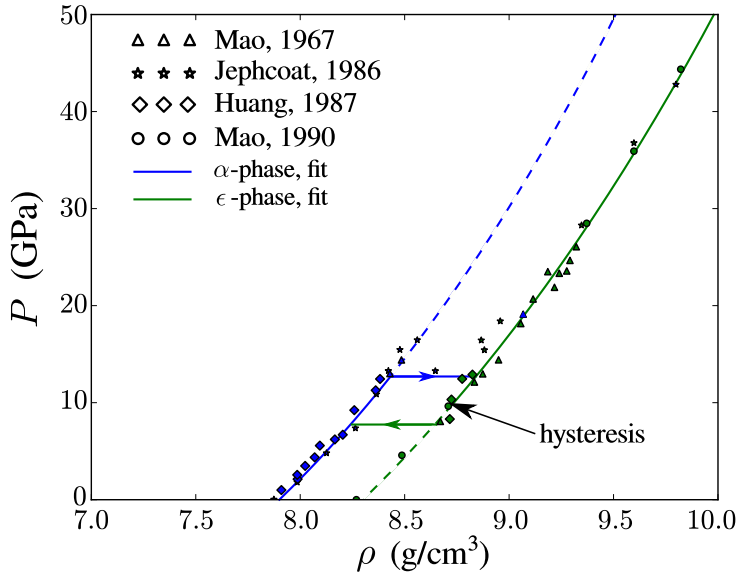

Figure 1. Equation of state of iron fitted to experimental data [7–11]. The α–ε phase transition is included with an appropriate hysteresis.

2. Iron and steel model

To fit the experimental data points the Mie–Grüneisen equation of state is used:

$$P - P_r = \gamma\rho(e - e_r), \tag{1}$$

where ρ is the density, e is the specific internal energy, P is the pressure, γ is the Grüneisen parameter, $e_r(\rho)$, $P_r(\rho)$ is the reference energy and pressure, respectively. The linear relation between the shock and mass velocities $u_s = c + su_p$, where c is the bulk sound speed in standard conditions and s is the coefficient, is a good approximation at compressions ($x = \rho_0/\rho < 1$) up to hundreds of GPa. In this case, the reference relationships are

$$P_r = \rho_0 c^2 \frac{1-x}{[1-s(1-x)]^2}, \qquad e_r = \frac{P_r}{\rho_0}\frac{1-x}{2}. \tag{2}$$

It is important to note that the reference pressure and energy are different for α and ε solid phases. In fact, they have different initial densities $\rho_{0\alpha}$ and $\rho_{0\varepsilon}$ (the corresponding compression ratios are $x_\alpha = \rho_{0\alpha}/\rho$ and $x_\varepsilon = \rho_{0\varepsilon}/\rho$), while other properties such as linear relationship between u_s and u_p are very close and require only a little adjustment:

$$P_{r\alpha}(x_\alpha) = \rho_{0\alpha} c^2 \frac{1-x_\alpha}{[1-s_\alpha(1-x_\alpha)]^2}, \qquad P_{r\varepsilon}(x_\varepsilon) = \rho_{0\varepsilon} c^2 \frac{1-x_\varepsilon}{[1-s_\varepsilon(1-x_\varepsilon)]^2}, \tag{3}$$

$$e_{r\alpha}(x_\alpha) = \frac{P_{r\alpha}}{\rho_{0\alpha}}\frac{1-x_\alpha}{2}, \qquad e_{r\varepsilon}(x_\varepsilon) = \frac{P_{r\varepsilon}}{\rho_{0\varepsilon}}\frac{1-x_\varepsilon}{2}. \tag{4}$$

The densities $\rho_1^{\alpha\varepsilon}$, $\rho_2^{\alpha\varepsilon}$ of the direct α–ε transition are defined using the well-known value for the corresponding pressure:

$$P_{r\alpha}(\rho_{0\alpha}/\rho_1^{\alpha\varepsilon}) = 13 \text{ GPa}, \qquad P_{r\varepsilon}(\rho_{0\varepsilon}/\rho_2^{\alpha\varepsilon}) = 13 \text{ GPa}. \tag{5}$$

The reverse ε–α transition appears at pressures lower than 13 GPa which is about 8.5 GPa [2]. The related densities $\rho_1^{\varepsilon\alpha}$, $\rho_2^{\varepsilon\alpha}$ are defined from similar equations:

$$P_{r\varepsilon}(\rho_{0\varepsilon}/\rho_1^{\varepsilon\alpha}) = 8.5 \text{ GPa}, \qquad P_{r\alpha}(\rho_{0\alpha}/\rho_2^{\varepsilon\alpha}) = 8.5 \text{ GPa}. \tag{6}$$

Table 1. Iron and steel parameters used in simulations.

Parameter name	Value
Initial α-phase density $\rho_{0\alpha}$, kg/m^3	7900
Initial ε-phase density $\rho_{0\varepsilon}$, kg/m^3	8300
Direct α–ε phase transition densities $\rho_1^{\alpha\varepsilon} \to \rho_2^{\alpha\varepsilon}$, kg/m^3	8440 $\to$ 8717
Reverse α–ε phase transition densities $\rho_1^{\varepsilon\alpha} \to \rho_2^{\varepsilon\alpha}$, kg/m^3	8550 $\to$ 8312
Specific heat capacity C_v, J/(kg K)	450
Grüneisen parameter γ	2.0
Bulk modulus B, GPa	165
Shear modulus G, GPa	83
Shock Hugoniot parameter c, m/s	4570
Shock Hugoniot parameter s_α	1.49
Shock Hugoniot parameter s_ε	1.40
Yield strength Y, GPa	0.5 (iron) and 1.5 (steel)
Tensile strength T, GPa	3.0

The direct and reverse transition boundaries are thus defined without thermal contribution to pressure which is a good approximation: this phase boundary is stable with the temperature growth up to $T \approx 900$ K [2]. The parameters of the equation of state are given in table 1.

Simulations of elastic-plastic flow in SPH are performed by evaluation of the stress deviator tensor $\hat{\mathbf{S}}$ with accounting of rotation using Hooke's law:

$$\dot{\hat{\mathbf{S}}} = 2G(\dot{\varepsilon} - \dot{\varepsilon} \otimes \mathbf{I}/3) - \dot{\mathbf{R}} \cdot \mathbf{S} + \mathbf{S} \cdot \dot{\mathbf{R}}, \tag{7}$$

where ε is the strain deviator tensor; G is the shear modulus; $\dot{\mathbf{R}}$ is the angular velocity tensor:

$$\dot{\mathbf{R}} = \left[(\nabla \otimes \mathbf{U})^{\mathrm{T}} - \nabla \otimes \mathbf{U} \right] /2. \tag{8}$$

The components of the volumetric strain rate tensor can be found from the Saint-Venant's compatibility condition:

$$2\dot{\varepsilon} - \nabla \otimes \mathbf{U} - (\nabla \otimes \mathbf{U})^{\mathrm{T}} = 0. \tag{9}$$

After that the stress deviator tensor $\hat{\mathbf{S}}$ is corrected to $\mathbf{S}$ via the von Mises criterion:

$$\mathbf{S} = \frac{Y}{\sigma_e}\hat{\mathbf{S}}, \qquad \text{if } Y < \sigma_e, \tag{10}$$

where Y is the yield strength; σ_e is the equivalent stress:

$$\sigma_e^2 = \frac{3}{2} S^{\alpha\beta} S^{\beta\alpha} = \frac{1}{2} \left\{ (S^{xx} - S^{yy})^2 + (S^{yy} - S^{zz})^2 + (S^{xx} - S^{zz})^2 + \right.$$
$$\left. + 6 \left[(S^{xy})^2 + (S^{xz})^2 + (S^{yz})^2 \right] \right\}. \tag{11}$$

The parameters for steel and iron are referenced in table 1.

3. Uniaxial plate impact compression

The typical scheme for plate impact simulation includes two samples: an impactor with the initial velocity towards the target. The impact produces shock waves which propagate to the bulk of both samples from the interface. The free surface velocity of the target is measured using VISAR and may be directly tracked in a simulation. As the shock reflects from the free

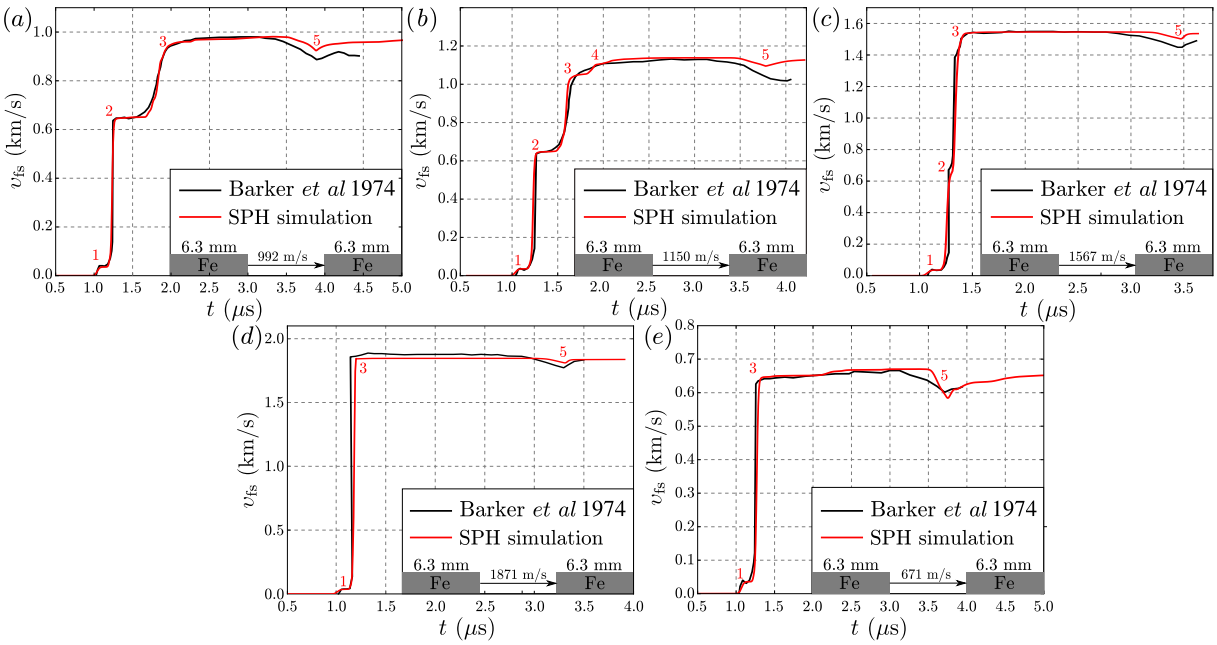

Figure 2. Simulated and experimental [5] wave profiles of tests 1 (a), 2 (b), 6 (c), 10 (d), and 13 (e). Each wave profile is marked with the following timestamps: 1—arrival of the elastic wave; 2—arrival of the wave front with direct α–ε phase transition; 3—arrival of the main pulse; 4—arrival of the wave reflected from phase boundary due to hysteresis; 5—spallation.

surface one can observe variations of its velocity with time which form the wave profile $U(t)$. The latter represents information about elastic-plastic and thermodynamic properties of materials: there are several parts of profile where each may be adjusted by a corresponding iron model parameter.

Numerical simulations are performed using our in-house three dimensional SPH software [12]. The problem setup is that the x-axis is placed along the direction of an impact, and corresponding sample lengths are in exact match with the experimental ones. About 10^3 particles are used along x-axis, while y and z contain only 15 particles with periodic boundary conditions. As a result, the obtained free surface velocities v_{fs} are compared to the experimental ones.

The model validation is performed using the tests 1, 2, 6, 10, 13, and 18 from [5]: it is enough to model the main features of wave profiles in iron at various load conditions. Both the impactor and target in all tests are iron samples about 6 mm in length, so that the shock propagation and release is symmetric. The results are presented in figure 2. Initially both the impactor and the target are in the α-phase. After the impact a set of waves is formed: the elastic precursor which reaches the free surface before other waves; the front of the direct α–ε phase transition, which is followed by the two-phase region; the main pulse, behind which all the material is already in the ε-phase. As the phase transition front reaches the free surface, the release wave induces the reverse phase transition in the bulk. Finally, the release waves from the main pulse in the target and the phase front reflection from the impactor provide the critical tension in the target, so that the spallation occurs near the interface between the impactor and the target.

The aforementioned scenario may vary due to the load intensity. For example, test 13 does not demonstrate that a complete transition from α to ε phase occurs. In contrast, heavy load results in almost instantaneous α–ε transition, so that the separate front with 13 GPa amplitude is not observed. The most interesting phenomena appear for the test 18 which is presented in figure 3 with the detailed x–t diagram: the hysteresis in the reverse α–ε transition is responsible

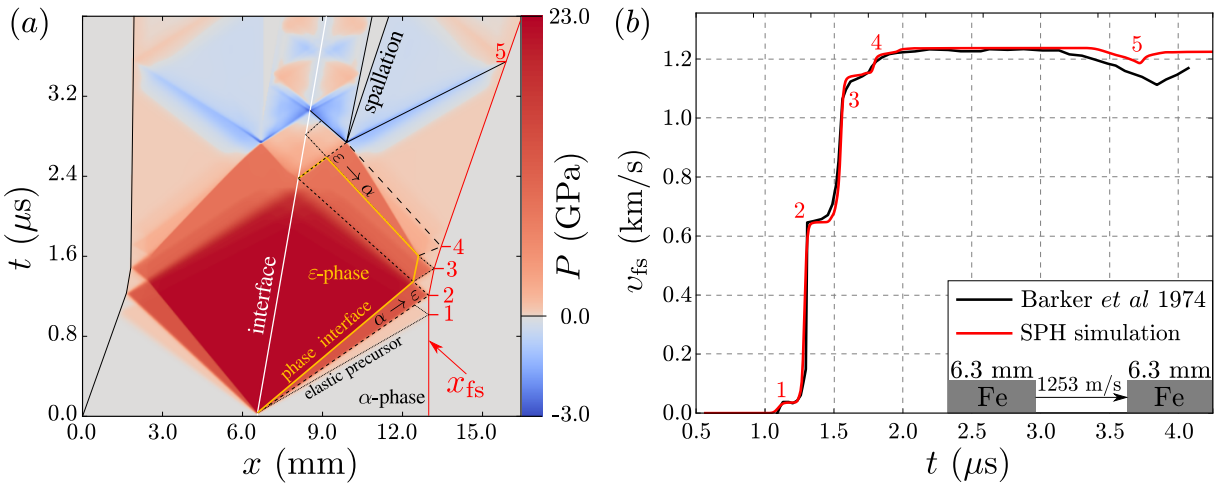

Figure 3. (a) x–t diagram with phase boundaries and schematic shock and rarefaction waves. (b) simulated and experimental [5] wave profiles of the test 18. The wave profile is marked with the following timestamps: 1—arrival of the elastic wave; 2—arrival of the wave front with direct α–ε phase transition; 3—arrival of the main pulse; 4—arrival of the wave reflected from phase boundary due to hysteresis; 5—spallation.

for part 3–4 of the wave profile. The presented analysis of simulation results demonstrates that elastic-plastic and thermodynamic properties of iron are important for adequate predictions at compressions up to 10–50 GPa. Such regime is usual during explosive compression of samples.

4. Uniaxial explosive compression

Similar to plate impact tests, the paper [13] provides wave profiles for spherical shells obtained using laser interferometer technique. In addition, it provides the photographs of saved samples which are useful to validate spallation. To reproduce precisely all the details of wave profiles we need a setup of explosive experiments with radial resolution of about 10^3 SPH particles. It is difficult to perform such simulation in three dimensions so that the problem is convenient to separate into two stages. First, the one dimensional simulation of explosively loaded iron sample, which length corresponds to the spherical shell width, is performed. The analysis of the resulting wave profile may help to adjust iron model parameters to better fit the specific steel used for spherical shells. To model tensile properties the radial resolution of shell width with about 100 particles is enough, so that simulations may be performed in a reasonable time of 3–4 hours on 128 processor cores with 15–20 millions of particles.

Here we perform the uniaxial loading of steel sample with the experimental length of 9.96 mm used in test 7 [13]. The plastic bonded explosive material PBX9404, which is used here, is simulated with the Lee–Tarver macrokinetic relations [14] and the Johnson–Wilkins–Lee (JWL) equation of state [15]. The detonation is induced by converting the inital high explosive (HE) material at the left side into the chemical products with the energy output. The results are presented in figure 4 in the form of x–t diagram and wave profile of the free surface velocity v_{fs}. The wave induced by detonation of PBX9404 has a triangular form, so that without spherical convergence the free surface velocity growth is not supported in contrast to experimental measurements. However, the width of pulse is enough to find out, that the phase front and the length of mixed phase region for steel is very close to one for the aforementioned iron. However, to model the elastic precursor the yield strength should be higher: about 1.5 GPa for this particular test.

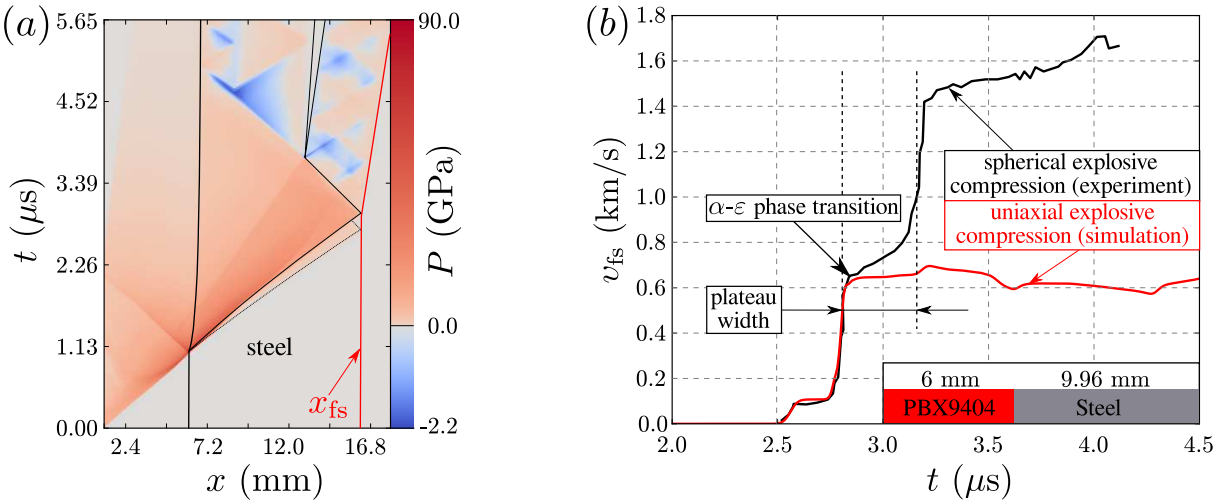

Figure 4. Uniaxial explosive compression with high spatial resolution: (*a*) x–t diagram of the process; (*b*) the simulated wave profile compared to one measured in the test 7 [13].

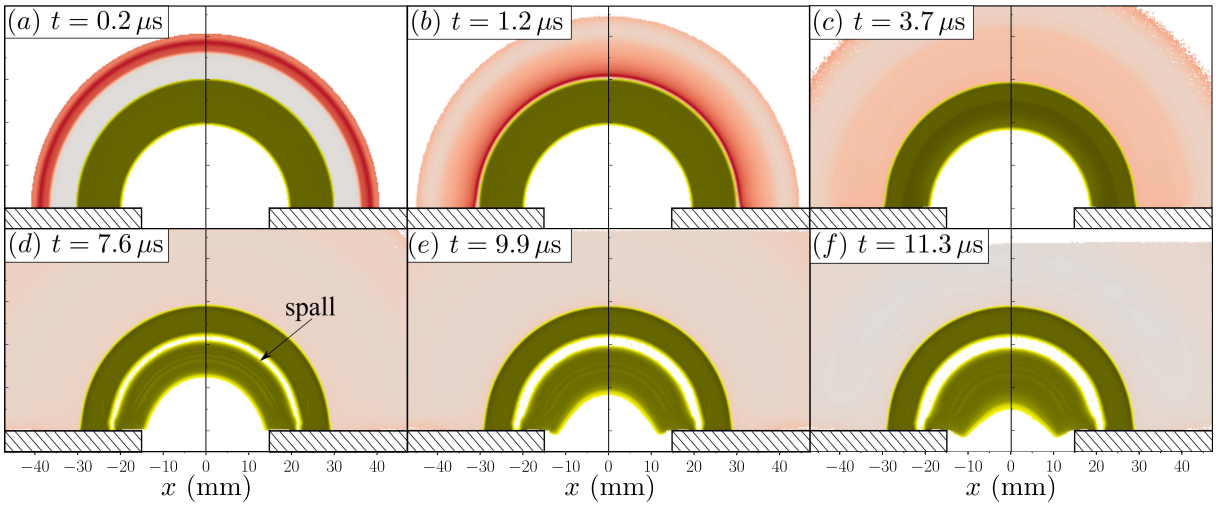

Figure 5. The evolution of steel shell under explosive compression with initial setup similar to the test 7 [13]. The yield strength of 1.5 GPa is used. Detonation of the HE layer (gray color) is initiated at $t = 0$ μs. Parts (*a*–*f*) are labeled with the corresponding timestamps. At $t = 7.6$ μs, the spallation of the inner iron layer (dark yellow color) occurs.

5. Spherical explosive compression

The evolution of a steel semispherical shell under explosive compression is simulated. Geometry of shells corresponds the test 7 [13]: the steel layer of 10 mm width surrounded by the HE layer of 10 mm width. Color maps of the diametral section of the steel shell under explosive compression are shown in figure 5, where yellow is used for steel and gray-red for HE. Initially, the thin layer of HE is transformed to products with the energy output. The detonation converges to the steel shell, propagates through it, and produces the spall at rarefaction. As a result, the steel shell splits into two parts. The outer shell becomes motionless, while the inner continues to converge.

6. Conclusion

We have developed the model for fluid dynamics simulations of iron and steel samples under plate impact and explosive compressions up to several tens of GPa. The model takes into account both elastic-plastic properties and the α–ε phase transition with hysteresis. The model for iron is validated on plate impact tests where all features of the wave profile are properly represented. Steel used in the explosive tests [13] seems to have higher yield strength, but the same thermodynamic properties as iron.

To model the behavior of iron at lower pressures, which are comparable to the yield strength magnitude, an adequate plasticity model is required. For higher compressions (hundreds of GPa) the linear relationship between the shock and material velocity at Hugoniot is rough, and better reference pressure approximation should be used.

Acknowledgments

This work has been done under financial support of program No. 2 of the Presidium RAS.

References

[1] Zepeda-Ruiz L A, Stukowski A, Oppelstrup T and Bulatov V V 2017 *Nature* **550** 492–5
[2] Kerley G I 1993 Multiphase equation of state for iron *Preprint* SAND93-0027 (Sandia National Laboratories)
[3] Bancroft D, Peterson E L and Minshall S 1956 *J. Appl. Phys.* **27** 291–8
[4] Duvall G E and Graham R A 1977 *Rev. Mod. Phys.* **49** 523
[5] Barker L M and Hollenbach R E 1974 *J. Appl. Phys.* **45** 4872
[6] Parshikov A N and Medin S A 2002 *J. Comp. Phys.* **180** 353–82
[7] Mao H K, Basset W A and Takahashi T 1967 *J. Appl. Phys.* **38** 272–6
[8] Andrews D J 1973 *J. Phys. Chem. Solids* **34** 825–40
[9] Jephcoat A P, Mao H K and Bell P M 1986 *J. Geophys. Res.* **91** 4477–684
[10] Huang E, Basset W A and Tao P 1987 *J. Geophys. Res.* **92** 8129–35
[11] Mao H K, Wu Y, Chen L C, Shu J F and Hemley R J 1990 *High Pres. Res.* **5** 773–5
[12] Egorova M S, Dyachkov S A, Parshikov A N and Zhakhovsky V V 2019 *Comput. Phys. Commun.* **234** 112–25
[13] Kozlov E A, Brichikov S A, Boyarnikov D S, Kuch'ko D P and Degtyarev A A 2011 *Fiz. Met. Metalloved.* **112** 412–28
[14] Lee E L and Tarver C M 1980 *Phys. Fluids* **23** 2362–72
[15] Kapila A K, Schwendeman D W, Bdzil J B and Henshaw W D 2007 *Combust. Theory Modell.* **11** 781–822